Chapter 6

Vanadium Oxide Cations

In this chapter, experimental as well as theoretical results on vanadium oxide cationic clusters are presented. The first section focuses on the theoretical results on VO^+ with an emphasis on the influence of the rare gas atoms He and Ar on the structure and vibrational frequency of VO^+. The second section presents the IRMPD spectra of selected oxygen rich vanadium oxide cluster cations, namely $(V_2O_5{}^+)_n$ $(n = 2, 3)$ and $V_3O_8{}^+$. These are the first successful experiments we performed at the FELIX facility.

6.1 Quantum computational results on VO^+ and $VO^+ \cdot R$ (R = He, Ar)

In this section, the computational results on VO^+ and $VO^+ \cdot R$ $(R = Ar, He)$ systems are presented. The first part of this section focuses on the theoretical results on VO^+. The calculations were performed with the DFT method and the B3LYP functional using the 6-311+G(d,p) basis set. These results are compared with other DFT calculations. Furthermore, the Morse potential approximation is used in order to determine the anharmonicity constant, which is further used in the calculation of the frequency for different vibrational levels. The second part of this section focuses on $VO^+ \cdot R$ $(R = Ar, He)$ complexes. The structure, binding energies and vibrational frequencies are determined using the multi-reference complete active space second order perturbation theory (MR-CASPT2) with the cc-pVXZ (X = 3, 4, 5) basis sets. The results are compared with DFT calculations. Based on these calculations, the influence of the rare gas atoms on the structure and vibrational frequency of the bare ion VO^+ are discussed. This section ends with the structure of $VO^+ \cdot Ar_2$.

6.1.1 Introduction and Motivation

Vanadium oxides are known for their catalytic properties such as in the production of sulfuric acid and for the reduction of the environmental pollution (e.g., reduction of NO with NH_3). Vanadium monoxide is the most studied system in the gas phase, experimentally as well as theoretically. Theoretical studies were mostly performed at the DFT level, by using a variety of basis sets and exchange-correlation functionals. Although a relatively good agreement with the experiment is observed when performing density functional calculations,[39,40] higher level studies on the bare vanadium monoxide cation stressed the multi-reference character of its ground state.[43,44] More accurate studies were performed by Pykavy *et al.*[44] who used multi-reference methods to determine the binding energies, bond distances and vibrational frequencies for $VO^{+/0/-}$. Recently, infrared VPD spectra were measured in our group for $VO^+ \cdot R$ ($R = H_2, He, Ar$).[39,41] The measured vibrational frequency of $1053 \pm 5\ cm^{-1}$ agrees well with the previously obtained value of $1060 \pm 40\ cm^{-1}$ for the bare ion VO^+.[138] A good match of the frequency is observed also with the multi-reference calculations of Pykavy *et al.*,[44] which predict the frequency of the VO^+ cation at 1058 cm^{-1}. The VPD experiments show small ($\pm$ 1 cm^{-1}) relative shifts of the band center by addition of one and two He atoms and one H_2 molecule. This indicates that the He and H_2 ligands have a negligible influence on the vibrational frequency of VO^+. A larger frequency shift is observed for the $VO^+ \cdot Ar$ system on the order of $+10\ cm^{-1}$ relative to the frequency of $VO^+ \cdot He$. The vibrational band of $VO^+ \cdot Ar$ presents additional structure at lower energies. In the hope to obtain more information on this large frequency shift in the $VO^+ \cdot Ar$ spectrum, high level calculations were performed. In these calculations not only structure and frequency analyses were performed, but also the dissociation energy was determined. The results of these calculations are presented in Subsection 6.1.4.

6.1.2 Methods and Basis Sets

For the calculations presented here, two quantum computational methods are used, namely the density functional theory (DFT) and the multi-reference complete active space second order perturbation theory (MR-CASPT2). In the DFT approach the energy of a system can be expressed as a functional of the electron density and there is no need for the knowledge of the wavefunction. For the DFT calculations, the

B3LYP[a] hybrid[b] exchange-correlation functional was used. B3LYP combines Hartree-Fock exchange with local-density approximation (LDA) exchange by the parameter c_0. It includes Becke's[139] gradient correction to LDA exchange which is scaled by c_X and the Vosko-Wilk-Nusair (VWN3) correlation, which can be corrected by the Lee-Yang-Parr (LYP)[140] correlation correction via the parameter c_C.[141]

$$E^{XC}_{B3LYP} = E^X_{LDA} + c_0(E^X_{HF} - E^X_{LDA}) + c_X \Delta E^X_{B88} + E^C_{VWN3} + c_C(E^C_{LYP} - E^C_{VWN3}) \quad (6.1)$$

These parameters were specified by Becke and were determined by fitting the atomization energies, ionization energies, proton affinities and first-row atomic energies in the G1 molecule set[142,143] ($c_0 = 0.20$, $c_X = 0.72$ and $c_C = 0.81$).

For the CASPT2[144] calculations, the complete active space self consistent field (CASSCF) approach[c] was used in order to obtain the multi-reference wavefunction. In the CASSCF method, a set of orbitals is chosen, referred to *active orbitals* with possible occupation numbers between 0 and 2. The space expanded by the active orbitals is referred to as *active space*. The other doubly occupied orbitals are called *inactive*. In this approach, the Hartree Fock (HF) wavefunction is used as reference in which only the molecular orbitals with the lowest energies are occupied and the remaining orbitals are unoccupied (virtual orbitals). The other determinants, which are included in the multi-reference wavefunction, are obtained by exciting electrons from the occupied orbitals to the virtual ones inside the active space. The CASPT2 method combines CASSCF with second order Rayleigh-Schrödinger perturbation theory. The efficiency of the CASPT2 method, with the use of CASSCF reference wavefunction, for the analysis of the low-energy electronic states in transition metal oxides has been demonstrated by de Graaf *et al.*[145] He showed that for an accurate description of the d shell, the active space must contain the $3d$ orbitals for the metal and the $2p$ orbitals from the ligand. In the case of VO^+, for an accurate description of the vanadium-oxygen bond, Pykavy *et al.*[44] showed the importance of including the $3d$ orbitals from vanadium and the $2p$ orbitals from the oxygen atom in the active space. In the CASPT2 calculations presented in Subsection 6.1.4, the same active space, as described by Pykavy *et al.* is used. The active space includes eight molecular orbitals ($8\sigma^2$, $3\pi^4$, $1\delta^2$ 9σ, 4π and 10 σ) and eight electrons (CAS(8,8)). For the $VO^+ \cdot Ar$

[a] Becke-style three parameter hybrid functional using the Lee-Yang-Parr correlation functional[139,140]

[b] B3LYP includes a certain amount of the Hartree-Fock exchange (exact exchange) and therefore it is referred to as hybrid functional.

[c] SCF - Self Consistent Field - It is an iterative process that is performed until the solution does not change from one iteration to the next.

calculations, a level shift was used in order to get read of the intruder states[d].

In some cases, in order to check the reliability of the CASPT2 results, calculations using the multi-reference averaged coupled-pair functional (MR-ACPF), developed by Gdanitz and Ahlrichs[146] method were performed. MR-ACPF yields energies close to full configuration interaction (full-CI)[e].

For the CASPT2 and ACPF calculations, the triple-ζ valenced polarized (TZVP) basis set developed by Ahlrichs *et. al.*[147,148] and the correlation consistent basis sets cc-pVXZ (X = 3, 4, 5) are used. For the vanadium atom, the cc-pVXZ (X = 3, 4, 5) basis sets were developed by Pykavy *et al.*[44] and for the oxygen and the rare gas atoms (Ar and He) by T. H. Dunning, Jr.[149] For the DFT/B3LYP calculations, the TZVP and the 6-311+G(d,p)[150,151] smaller basis sets are used.

One of the final aims of the studies presented here is the determination of the dissociation energy of the rare gas atoms from the VO^+ core. The dissociation energy is determined as follows:

$$D_e = E_{VO^+\cdot R} - E_{VO^+} - E_R \tag{6.2}$$

where D_e represents the dissociation energy and $E_{VO^+\cdot R}$, E_{VO^+}, E_R are the energies of the rare gas complex and of the fragments, respectively. The values obtained from equation (6.2) would be exact if the energies are calculated with the full-CI approach and with a complete basis set. Since the use of a complete basis set is not possible, truncations to the basis set must be made. These lead to errors in the dissociation energy value. One of this errors is the basis set superposition error (BSSE), where the orbitals from different atoms overlap and lead to an artificially improved description of the corresponding bond. In this thesis, the counterpoised correction (CP) of Boys and Bernardi[152] was used. The counterpoised corrected dissociation energy is expressed in equation (6.3), where the energies of the fragment ions were determined by using the geometry and the basis set of the parent ion.

$$D_e = E_{VO^+\cdot R} - E'_{VO^+} - E'_R \tag{6.3}$$

where E'_{VO^+} and E'_R are the counterpoised corrected energies of the fragments VO^+ and R, respectively. When the energy of one of the subsystems is evaluated, for example VO^+, the nuclear charge in atom R will be set to zero. By increasing the basis set, the error due to the basis set superposition can be reduced. Further improvements

[d] Virtual orbitals with energies close to the occupied orbitals which can intrude in the complete active space.

[e] Full-CI is a single reference method where all possible excitations of all electrons are considered. This approach combined with a complete basis set offers exact results.

to the value of the dissociation energy are obtained using an extrapolation to the basis set limit. Different functions have been proposed[153–155] for the extrapolation. In this work, the function proposed by Martin *et al.*[155] is used.

$$E = A + B/(l + 1/2)^4 + C/(l + 1/2)^6 \tag{6.4}$$

where l is the maximum angular momentum in the basis set and E is the molecular energy. Equation (6.4) represents the extrapolation function when the energy was calculated with three different correlation consistent basis sets.

6.1.3 The Vanadium Monoxide Cation VO^+

In order to gain more insight in the results obtained theoretically on $VO^+ \cdot He$ and $VO^+ \cdot Ar$, few calculations on the vanadium oxide cation were performed. The calculations were done with the Gaussian98 program package[156] using the DFT method with the B3LYP hybrid functional and the 6-311+G(d,p) basis set. These calculations predict an equilibrium bond distance of VO^+ of r_e = 1.54 Å, vibrational frequency ν = 1138 cm^{-1} and the BSSE corrected dissociation energy D_e = 5.6 eV[f]. The dissociation energy was calculated according to equation (6.5), where the numbers in the left upper corner of the atoms and molecule represent the multiplicity of the ground states of the atoms.

$$D_e(VO^+) = E(^3VO^+) - E(^5V^+) - E(^3O) \tag{6.5}$$

The value of the dissociation energy was corrected for the basis set superposition error using the counterpoised correction. As already discussed by Pykavy *et al.* the B3LYP values for D_0 of 5.53 eV underestimate by approximately 0.5 eV the experimental value of $D_0 = 6.09 \pm 0.28$ eV.[61,138]

Since VO^+ is a two atomic molecule, the Morse function can be used in order to approximate the value of the anharmonicity constant χ_e, by applying the formula (3.17) from Section 3.2. The obtained value of the anharmonicity constant is 0.006. The rather low anharmonicity shows that the VO^+ potential energy curve is very close at the bottom of the well to a harmonic potential. This results in a rather good evaluation of the vibrational frequencies for small amplitude oscillations by using the harmonic approximation, considering the fact that the anharmonicity is stronger noticeable at higher vibrational levels. The B3LYP harmonic vibrational frequency (1138 cm^{-1}) is considerably overestimated by approximately 70 cm^{-1} compared to

[f] Experimental values: r_{exp} = 1.56Å,[157] ν_{exp} = 1053 cm^{-1},[39] D_0 = 6.09 eV[61,138]

the experimental values of $1053 \pm 5\ cm^{-1}$. It is known that B3LYP frequencies are systematically too large. The overestimation is also due to the harmonic approximation, however for VO^+ the anharmonicity is very small (0.006), hence, in this case the overestimation is solely due to the method. To compensate for this, usually scaling factors are used for the B3LYP predicted frequencies.[39]

The knowledge of the anharmonicity constant is useful for the determination of the energies and frequencies of higher vibrational levels. These can be calculated by using the equations (3.18) and (3.19) from Section 3.2. The obtained values are listed in Table 6.1 where $\widetilde{\nu_e}$ is referred to as the harmonic frequency in cm^{-1} and the ΔE is the zero point energy $(1/2\hbar\omega^2)$.

Table 6.1: The values of the energy difference and frequencies determined for the first four vibrational levels by using the Morse potential approximation.

level (v)	e	$0 \rightarrow 1$	$1 \rightarrow 2$	$2 \rightarrow 3$	$3 \rightarrow 4$
Δ E [a.u.]	$2.58 \cdot 10^{-3}$	$5.12 \cdot 10^{-3}$	$5.05 \cdot 10^{-3}$	$4.98 \cdot 10^{-3}$	$4.925 \cdot 10^{-3}$
$\widetilde{\nu_v}$ $[cm^{-1}]$	1138	1124	1109	1095	1081

e - indicates values obtained at the equilibrium position

The results in Table 6.1 show that the (positive) anharmonicity causes a decrease of the energy difference between two successive vibrational levels with increasing v. As a consequence a red shift from the fundamental frequency for the higher vibrational transitions occurs, which makes multiphoton excitation difficult or even impossible.

6.1.4 Quantum Computational Results for the $VO^+ \cdot$ R (R = He, Ar) Complexes

In the following, the computational results on $VO^+ \cdot He$ and $VO^+ \cdot Ar$ using the multi-reference complete active space second order perturbation theory (CASPT2) are presented. The calculations were performed with the MOLPRO 2002.6 program package.[158]

Structural Analysis

The structures for VO^+, $VO^+ \cdot He$ and $VO^+ \cdot Ar$ at the CASPT2 level and the cc-pV5Z basis set, are presented in Figure 6.1. The calculations predict bent structures for the rare gas complexes with the rare gas atom attached to the vanadium. Tables

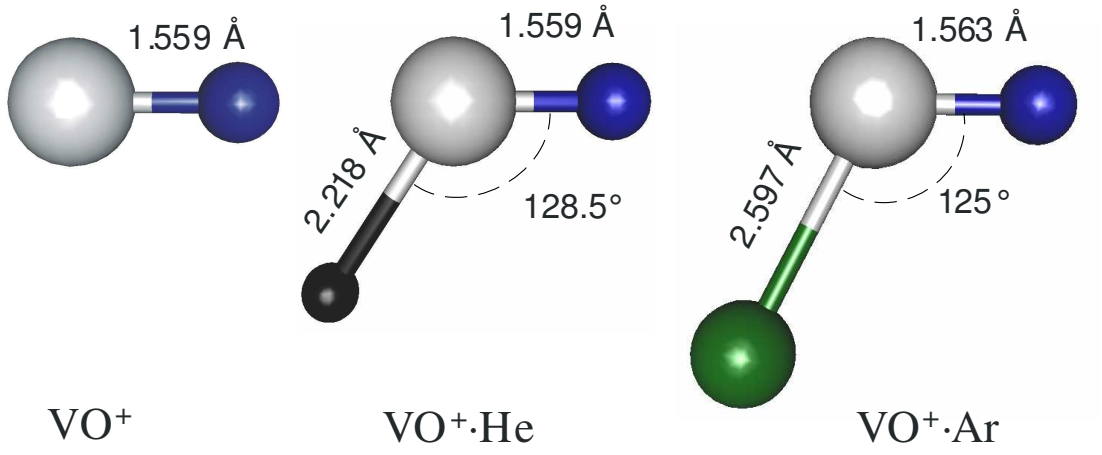

Figure 6.1: CASPT2 / cc-pV5Z structures for VO^+, $VO^+ \cdot He$ and $VO^+ \cdot Ar$. (O in blue, V in light gray, He in black and Ar in green)

6.2 and 6.3 list the CASPT2 / cc-pVXZ (X=3,4,5) inter-atomic distances for all three systems, as well as the $O - V - R_x$ angles. The distance r_e between the vanadium and the oxygen atoms at the cc-pV5Z basis set is approximately 1.56 $\AA$, in very good agreement with the experimental value of Harrington *et al.*[157] of $r_0 = 1.56$ $\AA$. With

Table 6.2: The inter-atomic distances for VO^+, $VO^+ \cdot He$ cations and the $He - V^+ = O$ angle values calculated by using the CASPT2 method with the cc-pVXZ (X = 3, 4, 5) basis sets.

Basis sets	VO^+	$VO^+ \cdot He$		
	r(VO^+) [Å]	r(VO^+) [Å]	$r(He \cdot V^+)$ [Å]	a($OV^+ \cdot He$) [°]
cc-pVTZ	1.5595	1.5598	2.2493	130.03
cc-pVQZ	1.5591	1.5595	2.2207	128.88
cc-pV5Z	1.5595	1.5599	2.2189	128.53

increasing basis set the values of the $V-O$ and $V-R_x$ distances and of the $V-O-R_x$ angles decrease slightly. The largest changes are observed in the $V - R_x$ (≈ 0.03 $\AA$) distance and in the angle 1.5°. At the cc-pV5Z basis set, for $VO^+ \cdot He$, the $V-O$ and the $V - He$ distances are 1.56 and 2.22 $\AA$, and the angle is 128.5°. For the $VO^+ \cdot Ar$ complex at the same basis set, the inter-atomic distances are larger, 1.563 $\AA$ for $V-O$ and 2.6 $\AA$ for $V - Ar$, whereas the angle is smaller and has a value of 125°, $\approx 3.5°$ smaller than for the He complex. The $V - O$ distance changes only slightly (0.0004 $\AA$ for $VO^+ \cdot He$ and 0.003 $\AA$ for $VO^+ \cdot Ar$) with the attachment of the rare gas atom.

In Table 6.4, a comparison between the DFT / B3LYP and CASPT2 geometry optimizations of the $VO^+ \cdot He$ molecule by using the TZVP basis set of Ahlrichs

Table 6.3: The interatomic distances in Angstrom (Å) and the angle values in degrees (°) calculated for $VO^+ \cdot Ar$ using the CASPT2 method with different basis sets.

Basis sets	VO^+	$VO^+ \cdot Ar$		
	r(VO^+) [Å]	r(VO^+) [Å]	$r(Ar \cdot V^+)$ [Å]	a($OV^+ \cdot Ar$) [°]
cc-pVTZ	1.5595	1.5621	2.6267	126.53
cc-pVQZ	1.5591	1.5622	2.6048	125.81
cc-pV5Z	1.5595	1.5629	2.5974	125.14

et al.[147,148] is presented. The DFT values are underestimated, by 0.15 $\AA$ for the vanadium-oxygen distance ($r_0^{exp} = 1.56$ $\AA$). The CASPT2 results at this basis set overestimate the inter-atomic distances (by 0.2 $\AA$ for the vanadium-oxygen). For the geometry optimization, by using the relatively small TZVP basis set, the B3LYP method seems to predict closer results to the experimental values than the CASPT2 approach.

Table 6.4: Comparison of the structure of $VO^+ \cdot He$ using the TZVP Ahlrichs basis set at the DFT and CASPT2 levels.

Method	VO^+	$VO^+ \cdot He$		
	r(VO^+) [Å]	r(VO^+) [Å]	$r(He \cdot V^+)$ [Å]	a($OV^+ \cdot He$) [°]
DFT	1.5464	1.5470	2.2187	126.67
CASPT2	1.5833	1.5835	2.3746	133.73

Investigation of the Dissociation Energies and Vibrational Frequencies

The structure calculations presented previously showed only slight changes due to the increase of the basis set. Larger influences are expected when energies are calculated, especially dissociation energies. For weakly bonded systems it is important to use corrections for the basis set superposition error, since for weak van-der-Waals interactions it can be on the same order of magnitude as the interaction energy. As previously mentioned, the basis set superposition error decreases with increasing the basis set. Table 6.5 and 6.6 shows the molecular and atomic energies calculated at the CASPT2 level with the three cc-pVXZ (X = 3, 4, 5) basis sets, as well as the BSSE corrected dissociation energy D_e of the He, respectively Ar atoms from the VO^+ chromophore. As can be observed from the two Tables 6.5 and 6.6, the values for the counterpoised correction (CP) for $VO^+ \cdot He$ decrease from 0.65 kJ/mol for the cc-pVTZ to 0.09 kJ/mol for the cc-pV5Z basis set. The same tendency is observed

also for the Ar complex, where the CP correction decreases from 2.48 kJ/mol for the cc-pVTZ basis set to 0.76 kJ/mol for cc-pV5Z. These BSSE errors represent less than 3% of the binding energy at the cc-pVQZ and cc-pV5Z basis sets, indicating that these basis sets are adequate for the calculation of such low binding energies. The last row in both Tables 6.5 and 6.6 shows the values of the molecular and atomic energies, as well as of the dissociation energy at the basis set limit, calculated with the extrapolation function developed by Martin *et al.*[155] The BSSE corrected and BSL extrapolated values of D_e are 9.43 kJ/mol (0.1 eV) for $VO^+ \cdot He$ and 42.29 kJ/mol (0.44 eV) for $VO^+ \cdot Ar$. The predicted dissociation energies are higher than calculated for other systems studied in this thesis, for example for $BrHI^- \cdot Ar$ with a CCSD(T) predicted dissociation energy of ≈ 0.04 eV.

Table 6.5: CASPT2 total energies in hartrees, the value of the counterpoised correction and the dissociation energies of the He atom in kJ/mol for $VO^+ \cdot He$. The last row shows the energies of the systems when extrapolating to the basis set limit (BSL) and the value of the dissociation energy at this limit.

Basis sets	VO^+	$VO^+ \cdot He$				
	E(VO^+)	E(He)	E(VO^+)	E($VO^+ \cdot He$)	CP	D_e
cc-pVTZ	-1017.84	-2.8943	-1017.85	-1020.74	0.649916	-5.79
cc-pVQZ	-1017.91	-2.8970	-1017.91	-1020.81	0.220122	-7.92
cc-pV5Z	-1017.92	-2.8980	-1017.93	-1020.83	0.092943	-8.54
BSL		-2.90	-1017.96	-1020.86		-9.43

Table 6.6: CASPT2 total energies in hartrees, the value of the counterpoised correction and the BSSE corrected dissociation energies of the Ar atom in kJ/mol for $VO^+ \cdot Ar$. The last row shows the energies of the systems when extrapolating to the basis set limit (BSL) and the value of the dissociation energy at this limit.

Basis sets	VO^+	$VO^+ \cdot Ar$				
	E(VO^+)	E(Ar)	E(VO^+)	E($VO^+ \cdot Ar$)	CP	D_e
cc-pVTZ	-1017.84	-527.01	-1017.84	-1544.87	2.48	-31.56
cc-pVQZ	-1017.91	-527.04	-1017.91	-1544.96	0.99	-37.79
cc-pV5Z	-1017.92	-527.05	-1017.92	-1544.99	0.76	-39.63
BSL		-527.06	-1017.95	-1545.03		-42.29

The dissociation energy at the basis set limit was calculated for only two basis sets as well. For the Ar complex, using the cc-pVTZ and cc-pVQZ basis sets, the BSL corrected dissociation energy has the value of 42.98 kJ/mol and for cc-pVQZ and cc-pV5Z 41.57 kJ/mol. The same calculations were performed for the He complex and

the values are 9.70 kJ/mol and 9.15 kJ/mol, respectively. These values are corrected for BSSE as well. The predicted high dissociation energies indicate that one photon is sufficient for the photodissociation of $VO^+ \cdot He$, but at least four photons are required for the dissociation of $VO^+ \cdot Ar$ at the experimentally observed band (1053 cm^{-1}).

Table 6.7: CASPT2 values for the frequency in cm^{-1} for $VO^+ \cdot He$ calculated by using the cc-pVTZ and cc-pVQZ basis sets. For comparison also the experimental stretching frequency for VO^+ is shown.

Basis sets	VO^+	$VO^+ \cdot He$		
	VO stretch	VO stretch	$V \cdot He$ stretch	$OV \cdot He$ bend
cc-pVTZ	1062.4	1066.9	201.9	56.7
cc-pVQZ	1051.8	1054.2	226	49.7
experimental	1060 ± 40 [a]	1053 ± 5 [b]		

[a] Reference;[138] [b] Reference[39]

Table 6.8: CASPT2 values for the frequency in cm^{-1} for $VO^+ \cdot Ar$ calculated by using the cc-pVTZ and cc-pVQZ basis sets. For comparison also the stretching frequency for VO^+ is shown.

Basis sets	VO^+	$VO^+ \cdot Ar$		
	VO stretch	VO stretch	$V \cdot Ar$ stretch	$OV \cdot Ar$ bend
cc-pVTZ	1062.4	1065.7	169.8	86.0
cc-pVQZ	1051.8	1053	190.7	72.8
experimental	1060 ± 40 [a]	1063 ± 5 [b]		

[a] Reference;[138] [b] Reference[39]

In order to investigate the influence of the attached rare gas atoms to the VO^+ chromophore on the infrared spectrum, a frequency analysis was performed at the cc-pVTZ and cc-pVQZ basis sets for both complexes. Tables 6.7 and 6.8 list the CASPT2 values for the vibrational frequencies calculated with both basis sets. The last rows in both tables show the experimental values of the vibrational frequency for VO^+ and for the rare gas complexes. A strong shift of more than 10 cm^{-1} in the predicted frequencies is observed when the basis set is increased from cc-pVTZ to cc-pVQZ. A weaker influence is expected when going to the cc-pV5Z basis set. However, these calculations were not performed due to the high costs requested for the frequency analysis. The influence on the frequency at the attachment of the rare gas atoms to VO^+ is small in the calculations and experiment. For the He complex a

shift of 2 cm^{-1} is predicted by the theory. This agrees well with the frequency shifts observed experimentally of approximately 1 cm^{-1}. In experiment a shift of $\approx +10$ cm^{-1} is observed for the Ar complex relative to $VO^+ \cdot He$ which is larger than the theoretically predicted shift (see Tables 6.7 and 6.8). The difference might be caused by the multiphoton process required in the experiment in order to measure the IR spectrum.

The last Table 6.9 presents the values of the dissociation energies and of the $V-O$ vibrational stretching frequencies performed at the B3LYP level by using the TZVP and the 6-311+G(d,p) basis sets. CP represents again the counterpoised correction. For comparison, the dissociation energy of the $VO^+ \cdot He$ complex was calculated using the TZVP basis set at the CASPT2 level as well. The BSSE corrected value is 4.4 kJ/mol which is much lower than the B3LYP dissociation energy of 9.46 kJ/mol. This indicates that the DFT binding energy of 9.46 kJ/mol, which is close to the BSSE corrected and BSL extrapolated CASPT2 value listed in Table 6.5, is probably caused by some error compensation. This comparison suggests that the DFT approach is not suitable for calculating so low binding energies.

Table 6.9: Comparison between the DFT dissociation energies and frequencies for the VO^+ stretch for the two systems $VO^+ \cdot He$ and $VO^+ \cdot Ar$, using the 6-311+G(d,p) and the TZVP basis sets. The energies are given in kJ/mol and the frequencies in cm^{-1}.

Basis sets	$VO^+ \cdot He$			$VO^+ \cdot Ar$		
	D_e	CP	VO stretch	D_e	CP	VO stretch
6-311+G(d,p)	-9.96	1.41	1138.46	-33.71	0.73	1133.19
TZVP	-9.46	0.9218	1126.11	-32.19	1.15	1121.74

Furthermore, the structure of the $VO^+ \cdot Ar_2$ was calculated using the CASPT2 approach and the cc-pVTZ basis set. These calculations predict that the second argon atom binds also on the vanadium side. Figure 6.2 shows the structure of this complex. No further studies were performed on this system due to the very time consuming calculations. The experiments performed in our group,[39] show the formation of complexes (in the case of He) with up to three rare gas atoms. Larger ones could not be detected, their absence suggesting a drop in the binding energy at addition of further rare gas atoms which dissociate previous to IR excitation due to CID in the trap. Future theoretical investigation of the dissociation energy at the attachment of a fourth rare gas atom to the VO^+ chromophore could verify this assumption. Calculations on the $VO^+ \cdot He_{2,3,4}$ are running and will be presented in a future article.

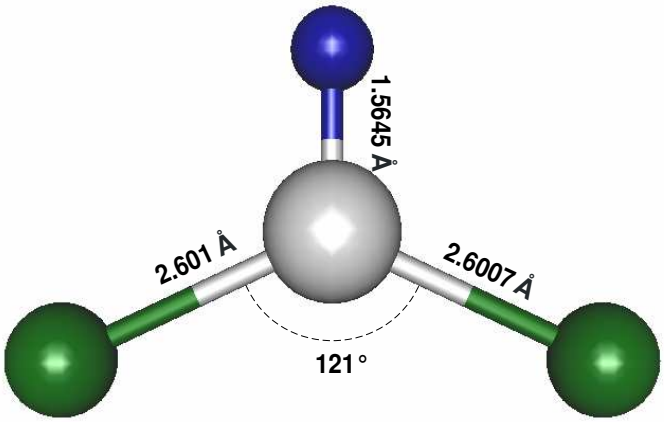

Figure 6.2: CASPT2 / cc-pVTZ structures for $VO^+ \cdot Ar_2$. (V- light gray sphere, O - blue sphere, Ar - green spheres.)

6.1.5 Conclusions

The structure, dissociation energies and vibrational frequencies for the rare gas complexes $VO^+ \cdot He$ and $VO^+ \cdot Ar$ were calculated in order to understand the influence of the rare gas atoms on the structure and vibrational frequency of the VO^+ core. The results were obtained from high level multi-reference CASPT2 calculation using different correlation consistent basis sets and were compared to VPD experiments performed in our group.[39] The calculations predict a bent structure for the two complexes. The BSSE and BSL corrected values of the dissociation energies are 9.43 and 42.29 kJ/mol (0.10 and 0.44 eV) for the He and the Ar complexes, respectively. These values are surprisingly high, especially for the Ar complex. The calculated dissociation energies predict that one photon is sufficient in order to reach the dissociation limit for the He complex, whereas for the Ar complex at least four photons are required for photodissociation at the experimentally measured band (1053 cm^{-1}). The vibrational analysis predicts a very good agreement for the frequency of $VO^+ \cdot He$ (1054 cm^{-1}) with the experiment (1053 cm^{-1}). The experimentally observed blue shift of 10 cm^{-1} for $VO^+ \cdot Ar$ from the frequency of $VO^+ \cdot He$ is higher than theoretically predicted shift. This difference might be caused by the multiphoton process required in the VPD experiments. Furthermore, the multi-reference results were compared to DFT calculations. The observed differences indicate that the DFT method is not suitable for calculating so low binding energies. The results presented here underline the importance of using high level methods for the calculation of molecular properties in some systems.

6.2 Vanadium Oxide Cations

In this section, the results on the IRMPD spectra of selected vanadium oxide cluster cations are presented. The systems discussed here are oxygen rich cluster cations. These experiments were the first successful experiments we performed at the FELIX facility. After a short introduction and description of the experiment, the results on $V_4O_{10}{}^+$ are presented. The IRMPD spectrum of $V_4O_{10}{}^+$ is the first published IR spectrum on vanadium oxide cations. The spectrum of $V_4O_{12}{}^+$ was measured as well in order to help the assignment of the $V_4O_{10}{}^+$ IR spectrum. In Subsection 6.2.4, the results on the IRMPD spectrum of $V_3O_8{}^+$ are presented. This section ends with the spectra of $V_6O_{15}{}^+$ and $V_6O_{13}{}^+$. Except for the IRMPD spectrum of $V_4O_{10}{}^+$, the result presented in this section will be published in future articles.

6.2.1 Introduction and Motivation

Vanadium oxides, especially V_2O_5 are known for their importance as catalysts in oxidation-reduction reactions,[28] as infrared active coatings[33] and sensors.[36] Many catalysts have vanadium oxide dispersed on different supports. The advantage of supported vanadium oxides lies in the variability of their geometric and electronic structure.[28] The characterization of their molecular structure is complicated by the different species which are formed upon deposition, e.g., isolated ions, polymeric species or mixed metal oxides with the support.[28] IR spectroscopy provides important information on the molecular structure, however surface vanadium oxide vibrations are often overlapped by IR bands of the support[28] and shifted or perturbed by the interaction with the support. Hence, investigation of the structure of vanadium oxide clusters in the gas phase, without the influence of the environment, offers important information.

The most studied vanadium oxide system in the gas phase is the diatomic vanadium monoxide,[159] which was found in the spectra of the metal-rich M-type stars[g]. Previous studies of the mass distribution[37] of vanadium oxide cations showed that the dominant peaks in the mass spectrum correspond to stoichiometries of $(VO_2)_n(V_2O_5)_m(O_2)_q{}^+$. Collision-induced dissociation (CID) experiments on vanadium oxide cations showed that VO_2, VO_3 and V_2O_5 are the main building blocks for most of these systems.[37] The formation as well as the reactivity with various reactants of isolated vanadium oxide cluster cations was extensively studied in the past years.[37,38,61,160–165] Based on CID and reactivity experiments, Bell *et al.*[37] pro-

[g]Red stars are classified as M-type. They have very cool surface temperatures below 3,500 K.

posed structures for some oxygen rich vanadium oxide cluster cations. However, these structures are in conflict with theoretical predictions.[39,40] The structure of vanadium oxide clusters was probed also by anion photoelectron spectroscopy. This method has proven useful for small systems, but the spectra of larger clusters are often too congested to resolve any vibrational structure.[159,166] Infrared spectroscopy in combination with quantum chemical calculations is one of the most direct and general applicable approach for the investigation of the structure of molecular systems. A systematic study of the structure of small vanadium oxide cations ($VO_x{}^+$ and $V_2O_x{}^+$) was performed in our group using the IR-VPD spectroscopy. These experiments, in combination with DFT/B3LYP studies (in collaboration with J. Sauer, Humboldt-Universität zu Berlin), succeeded in assigning structural and electronic properties to the measured features.[39] Based on these studies two characteristic frequency regions could be identified. The region below 900 cm^{-1} is characteristic for $V-O-V$ stretches and the region above 900 cm^{-1} for vanadyl stretches $V=O$.

Here, the IRMPD spectra of selected large vanadium oxide cluster cations is presented. Due to the high dissociation energies of vanadium oxide cations,[40] the IRMPD technique implies multiphoton absorption, which can make the experiments difficult and the spectra more complex. A more sensitive method is the messenger atom technique for which less photons are required for dissociation. However, the attachment of rare gas atoms is not possible for all systems. In these cases the IRMPD technique is advantageous for the measurements of the IR spectra.

6.2.2 Experiment

The vanadium oxide cations studied in this thesis were produced with the laser vaporization ion source, described in Chapter 2. The carrier gas consisted of 1% O_2 seeded in He. The FELIX radiation passed four $ZnSe$ optics, three windows and a lens with 500 mm focal length. Due to the low transmision of the $ZnSe$ material in the regions below 6 and above 16 μm (see Appendix B), the transmitted radiation intensity is reduced by more than 50% in these ranges. The FELIX macropulse energy was 50-60 mJ and the bandwidth of the laser was less than 1% of the central frequency.

6.2.3 IRMPD Spectra of $V_4O_n{}^+$ (n = 10, 12) Cations

The IRMPD spectrum of $V_4O_{10}{}^+$ represents the first published infrared spectrum on vanadium oxide cations.[167] The results were presented in detail in the diploma

thesis of G. Santambrogio.[47]

The IRMPD spectrum of $V_4O_{10}{}^+$ was measured between 600 and 1700 cm^{-1}. The spectrum in the range from 610 to 1425 cm^{-1} is shown in Figure 6.3, where the $V_4O_8{}^+$ (O_2-loss) ion signal yield, formed by photodissociation of $V_4O_{10}{}^+$ in the trap, is plotted as a function of the FELIX photon energy. This spectrum was measured with

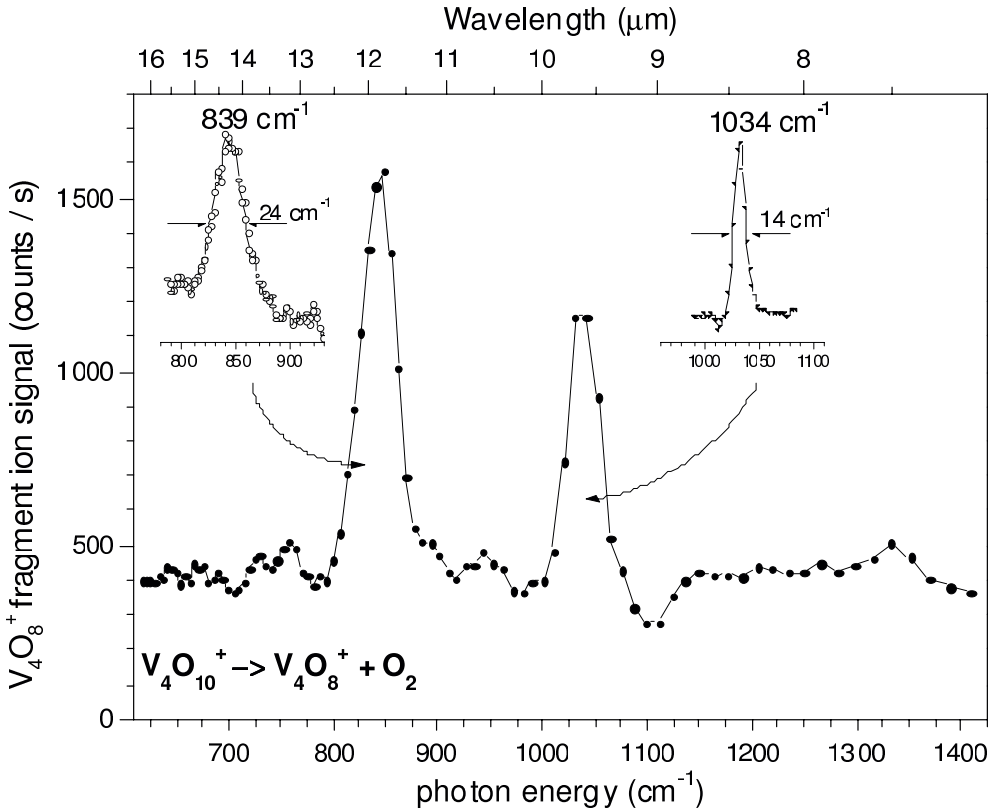

Figure 6.3: The gas phase IRMPD spectrum of the $V_4O_{10}{}^+$ cation measured with a step of 0.1 μm. The single fragmentation channel is the loss of one O_2 molecule. The $V_4O_8{}^+$ fragment ion signal is monitored as a function of the FELIX frequency. The insets show high resolution spectra recorded for each band (step = 0.02 μm).[167]

0.1 μm step size. In Figure 6.3, a background signal of $\approx$ 400 $counts/s$ is observed, which was formed by CID with the cold He atoms in the trap. The spectrum reveals two peaks at 839 and 1034 cm^{-1}. Tuning the laser to the resonant frequencies, no other fragmentation channels are observed than the O_2-loss or loss of two O-atoms. The present experimental setup cannot distinguish between these two fragmentation channels. Higher resolution spectra with 0.02 μm step size were measured over the region with infrared activity (see the insets of Figure 6.3). The widths of the two peaks are 24 and 14 cm^{-1}. The width of the first band is larger that the FELIX bandwidth ($\approx$ 1% of the central frequency) and might cover additional unresolved

bands. No other peaks outside the presented range were observed.

Collision induced dissociation (CID) experiments performed by Bell *et al.*[37] showed that collisions of the $V_4O_{10}{}^+$ cation with Xe atoms lead to dissociation of one O_2 molecule already at thermal energies. Other fragmentation channels are observed only at collision energies higher than 3 eV. The same behavior was observed in the photodissociation with 532 nm radiation experiments of Kooi *et al.*[168] Both these studies suggest a structure for $V_4O_{10}{}^+$ which consists of a $V_4O_8{}^+$ core with an additional O_2 unit attached. From the CID experiments[37] it is difficult to estimate the bond dissociation threshold of the O_2 molecule because the internal energy of the ions is unknown. In our experiment, the clusters formed by the laser vaporization source are "hot". Their internal temperature is often controlled by an evaporative cooling mechanism and by the free expansion as the ions leave the source. Possible collisions with He atoms (which have room temperature) will also lead to heat exchange. At the entrance in the trap, the internal energy of the clusters is close to but lower than the energy necessary to break the weakest bond. After entering the trap, the clusters will either dissociate through collisions with He atoms or will be thermalized to the ambient temperature (<70 K). An evidence for the dissociation is observed in the background signal of the infrared spectrum of Figure 6.3.

No simulation of the infrared spectra for $V_4O_{10}{}^+$ which could help the assignment of the measured IRMPD spectrum exist to date in the literature. There are however, predictions of the structure of few low lying isomers which were calculated by Bonačić-Koutecký *et al.* using the DFT/B3LYP method.[38] These calculation predict a cage type structure for the lowest lying isomer. The simplicity of the measured IRMPD spectrum suggests a structure with a high symmetry, possibly, for example, a cage type geometry. A cage type structure was predicted by Vyboishchikov and Sauer as well for the lowest lying neutral V_4O_{10} isomer. They also simulated the IR spectra for this isomer as well as for additional few neutral V_4O_{10} isomers.[169] Comparing the experimental IRMPD spectrum of the cation with the simulated spectra of the neutral V_4O_{10} isomers, a good overlap with the lowest energetically lying isomer (labeled as TETRA in Ref.[169]) is observed. Its IR spectrum reveals two bands at $\approx$ 800 and 1080 cm^{-1} close to the experimentally observed peaks (839 and 1034 cm^{-1}). Based on these investigations as well as on previous studies on small vanadium oxide cations,[39] the two bands observed in the IRMPD spectrum at 839 cm^{-1} and 1034 cm^{-1} can be assigned to $V-O-V$ antisymmetric stretch and to $V=O$ stretch, respectively.

In our publication, a weakly bound $V_4O_8{}^+ \cdot O_2$ adduct was proposed as the absorbing species and not the most stable, covalently bound cage type $V_4O_{10}{}^+$ isomer.

This tentative assignment was in part based on the observed single dissociation product, namely $V_4O_8{}^+$ (O_2-loss channel).[167] One such isomer of the type $V_4O_8^+ \cdot O_2$ was calculated by Bonačić-Koutecký,[38] but its IR spectrum was not published.

In our article[167] it was also stated that the IRMPD technique is limited to systems with moderately low dissociation energies (1-2 eV), considering that the absorption of a high number of photons required to overcome dissociation energies higher than 2 eV is less probable. In light of the recent experiments on the vanadium oxide anions[42] with dissociation energies of up to 6 eV[170] this prediction seems questionable and the assignment to a cage type structure which does not necessarily contain a weakly bound O_2 is feasible. For such a system the fragmentation of an O_2 unit is expected to require high dissociation energies. This suggests that no or low CID dissociation should be observed in the trap. In our experiment, the observed background signal formed through CID represents 25 % of the fragment ion measured at the maximum of the peak with the highest intensity. Thus, if the lowest lying isomer of $V_4O_{10}{}^+$ would be the absorbing specie, then the observed CID background is unexpected.

In the hope to obtain more information which could help the structural identification of $V_4O_{10}{}^+$, the IRMPD spectrum of $V_4O_{12}{}^+$ was measured between 600 and 1600 cm^{-1}. Figure 6.4 shows the IRMPD spectrum of $V_4O_{12}{}^+$ in the range from 680 to 1170 cm^{-1}. No other peaks outside the presented range are observed. The spectrum was measured with 0.1 μm step size. A background signal of $\approx$ 1500 counts/s is formed through CID with the He atoms in the trap. Higher resolution spectra measured with 0.02 μm step size are shown in the inset of Figure 6.4. At least five bands centered at 792, 836, 845, 867 and 1042 cm^{-1} are observed. The width of the last peak is 19 cm^{-1}, larger than the bandwidth of the laser and might be caused by additional unresolved bands. The spectrum of $V_4O_{10}{}^+$ is shown in Figure 6.4 (open circles) as well. The two spectra are very similar, except for the third band at 792 cm^{-1}, which is observed only in the IR spectrum of $V_4O_{12}{}^+$.

This cation presents many fragmentation channels namely the loss of one O_2 molecule, O_3-loss, the loss of two O_2 molecules and one VO molecule loss. The O_2-loss spectrum reveals the most intense bands, followed by $2O_2$-loss channel, O_3 and VO-loss. Photodissociation experiments with 532 nm radiation[168] show evidence for the dissociation of O_2 and two O_2 molecules at low fluences. At higher fluences, formation of VO_2 (V_3O_{10}-loss) and VO (V_3O_{11}-loss) is observed, however no VO-loss could be detected. Figure 6.5 shows the IRMPD spectra of the O_2 and $2O_2$-loss channels. The relative peak intensities in the $2O_2$-loss spectrum are different than in the O_2-loss spectrum. The presented spectra in Figure 6.5 were measured with different FELIX

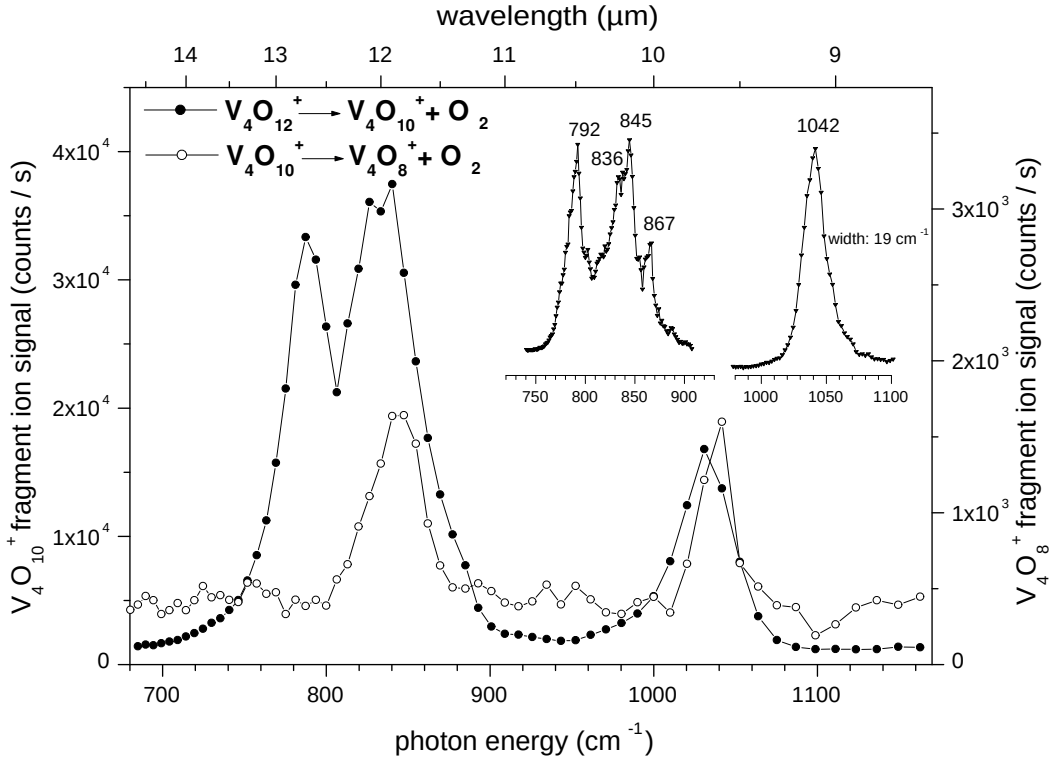

Figure 6.4: The IRMPD spectrum of the $V_4O_{12}{}^+$ cation. The $V_4O_{10}{}^+$ fragment ion signal was measured as a function of the laser frequency (closed circles). The insets present high resolution spectra of each peak measured with a lower step size and on a smaller frequency range. For comparison, the spectrum of the $V_4O_{10}{}^+$ cation is shown as well (open circles).

pulse energies (46 mJ and 60 mJ for the O_2-loss and $2O_2$-loss spectra). When the two fragmentation channels are measured with the same FELIX pulse energy, both spectra show similar relative peak intensities as in the lower panel of Figure 6.5. Hence, the difference in the relative peak intensities between the two spectra is attributed to different FELIX pulse energies used for the experiments. The fragment ion yield in the $2O_2$-loss spectrum is eight times lower than in the O_2-loss spectrum, suggesting a sequential dissociation mechanism:

$$V_4O_{12}^+ \rightarrow V_4O_{10}^+ + O_2 \rightarrow V_4O_8^+ + 2O_2$$

The $2O_2$-loss spectrum reveals only two bands at 823 and 1039 cm^{-1}, however the first band has a large width that might cover two unresolved bands similar to the first two peaks in the O_2-loss spectrum. The similarity of the $V_4O_{12}{}^+$ and $V_4O_{10}{}^+$ spectra suggests that the structure of $V_4O_{12}{}^+$ contains a $V_4O_{10}^+$ core with one O_2 attached to it. The simplicity of the IRMPD spectra of $V_4O_{12}{}^+$ suggest a high symmetry structure, possibly similar to the cage type structure proposed for $V_4O_{10}{}^+$. The richer

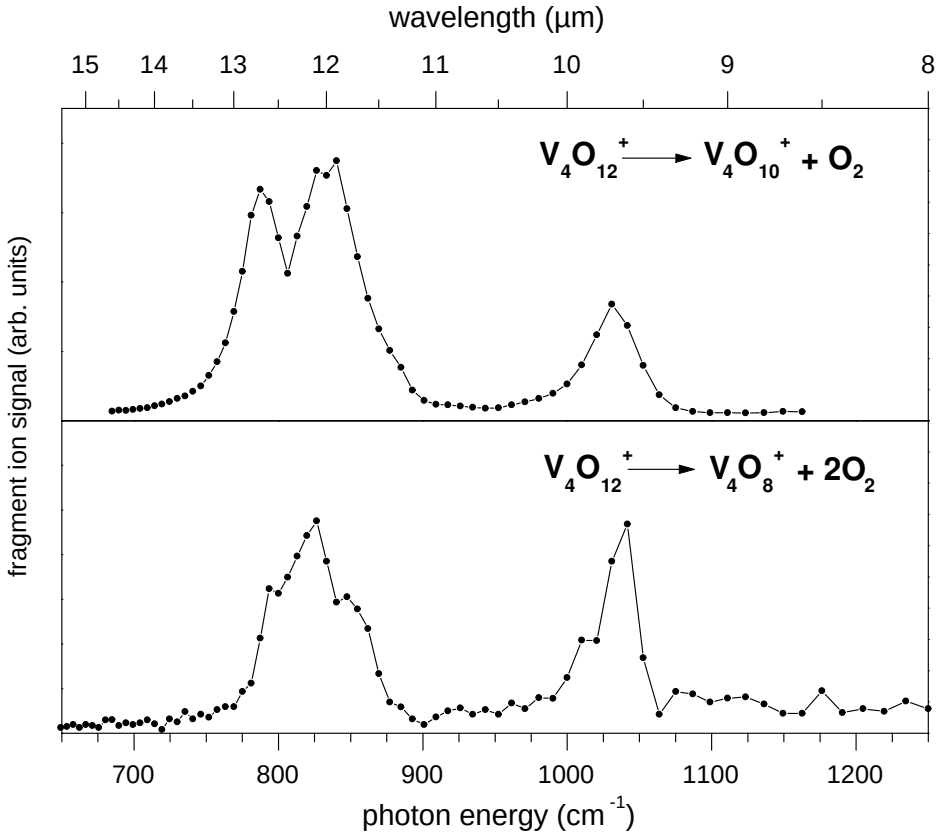

Figure 6.5: The IRMPD spectrum of O_2 and $2O_2$-loss fragmentation channels of $V_4O_{12}{}^+$. The spectrum of the O_2-loss channel was measured with 0.05 μm steps and the $2O_2$-loss spectrum with 0.1 μm step size.

vibronic pattern measured for $V_4O_{12}{}^+$ compared to $V_4O_{10}{}^+$ (see Figure 6.4) might be possible to explain by the breaking of symmetry due to the additional O_2 group. The reason that the band at 1042 cm^{-1} in $V_4O_{12}{}^+$ does not separate at O_2 addition might be caused by the binding of O_2 to the frame of the structure and not to the vanadyl. In this case the $V = O$ mode might not influenced by the presence of the weakly bound O_2. Since there are no calculations for the $V_4O_{12}{}^+$ cluster cation, the interpretation of the spectrum is difficult. It is possible that another structure with weakly bound O_2 units is probed in the experiment. However, the IRMPD spectrum of $V_4O_{10}{}^+$ agrees well with the IR spectrum of the neutral lowest lying isomer (called TETRA), suggesting a similar structure for the cation. The similarity of the $V_4O_{10}{}^+$ and $V_4O_{12}{}^+$ spectra supports this tentative assignment. However, the origin of the CID background observed for $V_4O_{10}{}^+$ remains still unexplained.

In conclusion, the IRMPD spectrum of the $V_4O_{10}{}^+$ cation was measured between 600 and 1700 cm^{-1}. The single dissociation channel is the O_2-loss. The spectrum

Table 6.10: Peak positions for multiphoton dissociation of $V_4O_{12}^+$ and $V_4O_{10}^+$.

parent ion	fragment ion	position (cm^{-1})
$V_4O_{12}^+$	$V_4O_{10}^+$	792, 836, 845, 867, 1042
	$V_4O_8^+$	823, 1039
$V_4O_{10}^+$	$V_4O_8^+$	839, 1034

reveals two peaks at 839 and 1034 cm^{-1} which were assigned based on previous experimental and theoretical studies on smaller vanadium oxides[39] to the $V-O-V$ and $V=O$ modes. Based on the comparison of the IRMPD spectrum of $V_4O_{10}^+$ to the simulated IR spectrum of neutral V_4O_{10}[169] a tentative assignment to the lowest lying isomer is proposed. The observed CID background remains difficult to explain. This assignment is supported by the similarity of the IRMPD spectra of $V_4O_{12}^+$ and $V_4O_{10}^+$. The richer vibronic pattern in $V_4O_{12}^+$ is attributed to possible symmetry breaking of the $V_4O_{10}^+$ cage type structure at the addition of O_2 unit.

6.2.4 IRMPD Spectra of $V_3O_8^+$ Cations

Figure 6.6 (lower panels) shows the IRMPD spectrum of the $V_3O_8^+$ cation measured in the range from 600 to 1100 cm^{-1}. Two fragmentation channels are observed, O-loss and O_2-loss. In photofragmentation[168] and CID[37] experiments, only O_2-loss was observed at low energies. At higher energies other fragmentation channels are observed as well, however, the CID experiments show no evidence for O-loss.

The O_2-loss spectrum shown in Figure 6.6 (middle panel) reveals a very intense peak at 1036 cm^{-1}. Five additional bands at 633, 727, 752, 817 and 852 cm^{-1}, fifty times weaker, are observed in the lower energy part of the spectrum. $V_3O_8^+$ is the only studied system which presents such a strong intensity difference between the band at $\approx$ 1040 cm^{-1} and the other peaks. The relative peak intensities in the O-loss spectrum are different (see Figure 6.6, lower panel). Two intense peaks at 841 and 1036 cm^{-1} are observed. The peak at 841 cm^{-1} is very broad and might cover additional unresolved bands. An additional weak feature is observed at 743 cm^{-1}. No band at $\approx$ 630 cm^{-1} is observed for this fragmentation channel. Peaks at $\approx$ 630, 740, 840 and 1040 cm^{-1} are characteristic for many vanadium oxide cluster cations.[39] Based on previous experimental and theoretical studies,[39,167,169] the bands below 900 cm^{-1} are assigned to $V-O-V$ modes and the bands at $\approx$ 1040 cm^{-1} to the vanadyl stretch. Since the spectra are so different, the two fragmentation channels observed for $V_3O_8^+$ might result from the photodissociation of two different isomers and not

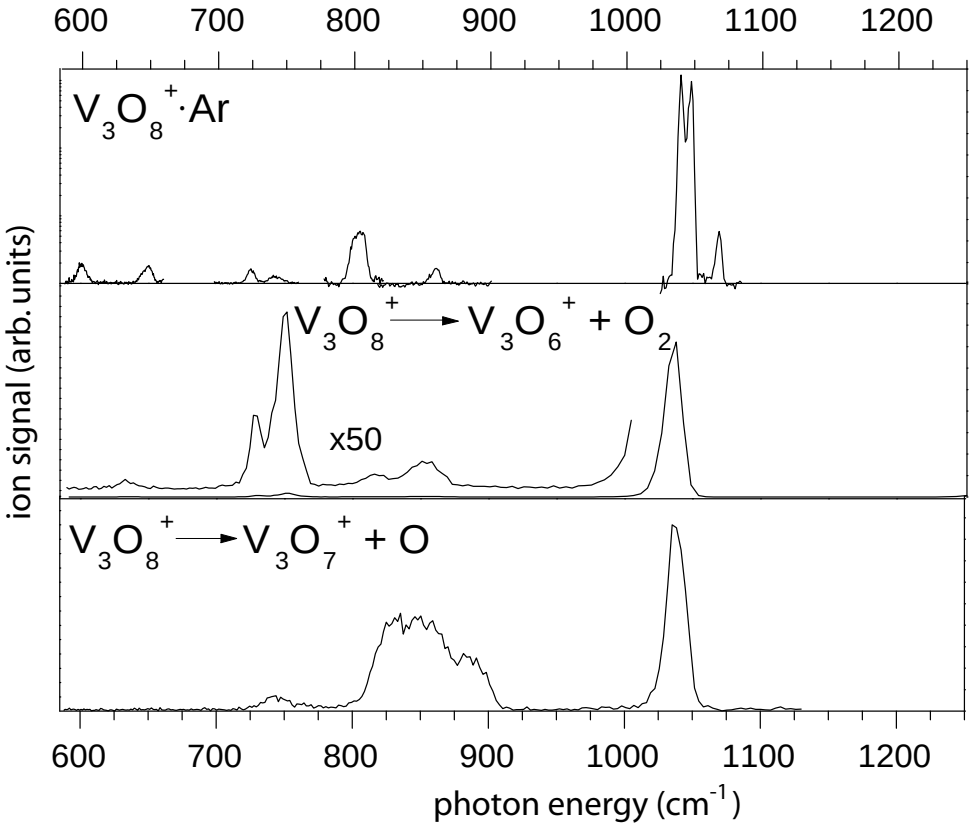

Figure 6.6: The VPD and the IRMPD spectra of $V_3O_8{}^+$.

from sequential dissociation:

$$V_3O_8^+ \rightarrow V_3O_7^+ + O \rightarrow V_3O_6^+ + O + O \tag{6.6}$$

The IR spectrum of the $V_3O_8{}^+$ cation was measured in our group with the messenger atom technique as well, where Ar was used as spy atom (see Figure 6.6, upper panel).[49] The VPD spectrum of the $V_3O_8^+ \cdot Ar$ complex reveals nine bands in the region from 600 to 1070 cm^{-1}. The positions of the bands are listed in Table 6.11. The IRMPD and VPD spectra are similar, but not identical. The number of the peaks in the IRMPD spectra of both fragmentation channels is smaller than in the VPD spectrum. The peaks at 725, 743, 805, 861 1042 and 1049 cm^{-1} in the VPD spectrum are close to the bands at 727, 752, 817, 852 and 1036 cm^{-1} observed in the O_2-loss IRMPD spectrum. The O-loss spectrum reveals broad features centered at 743 and 852 cm^{-1} which might cover unresolved bands close to the ones observed in the VPD spectrum at 725 and 743 cm^{-1} and at 805 and 861 cm^{-1}, respectively. The VPD spectrum reveals additional bands located at 601, 649 and 1069 cm^{-1}. These

peaks are not observed in any of the IRMPD spectra corresponding to the two fragmentation channels. The fact that peaks at low energies are not well observed in the IRMPD spectrum is not so surprising since a higher number of photons is necessary to be absorbed in this range in order to reach the dissociation threshold. Only one very weak peak at 633 cm^{-1} is observed in the O_2-loss spectrum, which does not appear in the other two spectra. The relative peak intensities in the VPD and IRMPD spectra are also different, especially for the O_2-loss spectrum. The relative intensities fit better in the VPD spectrum with the O-loss spectrum. It is possible that the VPD and the O-loss spectra result from the same isomer, whereas the O_2-loss spectrum might result from a different isomer. However, the absence of the band at 1069 cm^{-1} in the IRMPD spectra remains an open issue.

Table 6.11: Experimentally determined vibrational frequencies (cm^{-1}) from IRMPD and VPD[a] spectra.

Parent Ion	Fragment Ion	Band Position
$V_3O_8{}^+$	$V_3O_7{}^+$	743, 852, 1036
$V_3O_8{}^+$	$V_3O_6{}^+$	633, 727, 752, 817, 852, 1036
$V_3O_8^+ \cdot Ar$	$V_3O_8{}^+$	601, 649, 725, 743, 805, 861, 1042, 1049, 1069

[a] - Results presented in the diploma thesis of O. Gause[49]

In conclusion, the IRMPD spectra of the $V_3O_8{}^+$ cation was measured for the first time at the FELIX facility between 600 and 1700 cm^{-1}. Two fragmentation channels with different spectra are observed. The difference in the two spectra suggests that the structure of two isomers was probed in the experiment. Based on previous DFT calculations on smaller vanadium oxide cations, the bands below 900 cm^{-1} are assigned to the $V-O-V$ stretches, whereas the bands above 900 cm^{-1} are assigned to the $V=O$ mode. The experimental results were also compared to existing VPD experiments. Comparison of the spectra suggests that the VPD and the O-loss IRMPD spectra might result from the same isomer, whereas the O_2-loss spectrum might result from a different isomer. A structural assignment to the tentatively predicted isomers could be obtained from theoretical calculations which will be hopefully stimulated by the experiments presented here.

6.2.5 IRMPD spectra of $V_6O_n^+$ (n = 13, 15) Cations

The IRMPD spectrum of $V_6O_{15}{}^+$ was measured in the region from 600 to 1600 cm^{-1}. The spectrum in the range from 800 to 1075 cm^{-1}, measured with 0.02 μm step size is shown in Figure 6.7. Two dissociation channels are observed: O_2-loss and

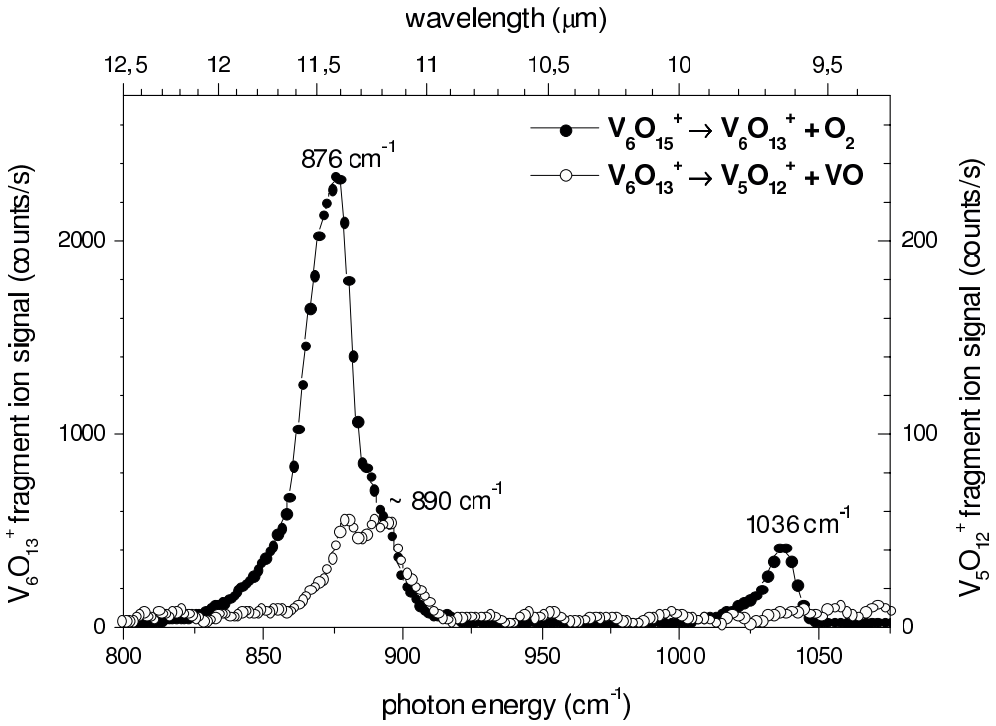

Figure 6.7: The IRMPD spectrum of the $V_6O_{15}{}^+$ cation. Two fragmentation channels are shown, the second producing much less intense absorption bands.

VO_3-loss. CID experiments performed by Bell *et al.*[37] measured also two dissociation channels with the O_2-loss as main fragmentation channel, followed by VO_3-loss. In Figure 6.7, the $V_6O_{13}{}^+$ ion signal intensity (O_2-loss) is plotted on the left axes (black dots), whereas the $V_5O_{12}{}^+$ ion signal intensity (VO_3-loss) is plotted on the right axes (open circles). The O_2-loss spectrum reveals two peaks at 876 and 1036 cm^{-1}. The second band has a smaller intensity (6 times) than the peak at 876 cm^{-1}, in contradiction to most of the studied vanadium oxide cluster cations, where the peak at 1036 cm^{-1} had the highest intensity. The fragment intensity at the maximum of the peak located at 876 cm^{-1} represents only 12 % of the parent ion signal. The VO_3-loss spectrum reveals only one weak band at 890 cm^{-1}. The intensity of this absorption band is 30 times weaker than in the O_2-loss spectrum. A second band at ≈1036 cm^{-1} cannot be observed. This can be due to the low intensity this peak would have if the same relative intensities are considered as in the O_2-loss spectrum.

A sequential dissociation mechanism could explain the two observed channels:

$$V_6O_{15}^+ \rightarrow V_6O_{13}^+ + O_2 \rightarrow V_5O_{12}^+ + O_2 + VO \tag{6.7}$$

where first the $V_6O_{13}{}^+$ ion signal is formed by photodissociation, which further absorbs energy and fragments to form $V_5O_{12}{}^+$. Only a low background signal (few $counts/s$) formed by CID dissociation with the cold He atoms in the trap is observed, indicating a high dissociation energy.

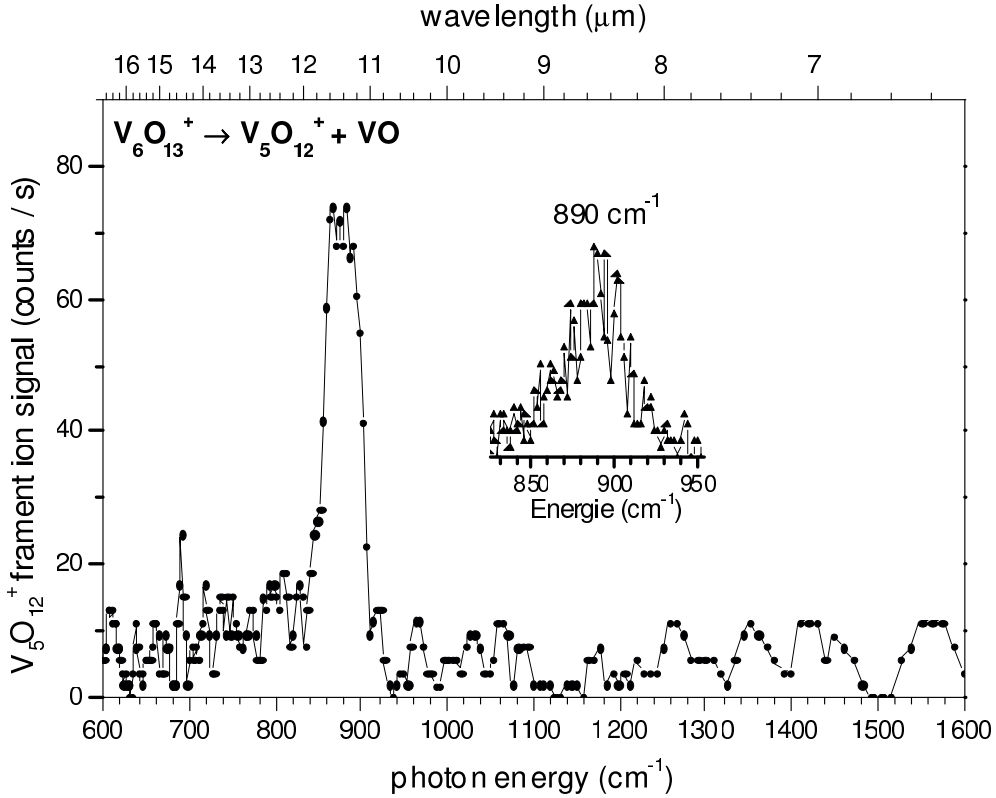

Figure 6.8: The IRMPD spectrum of the $V_6O_{13}{}^+$ cation. The $V_5O_{12}{}^+$ fragment ion signal is monitored as a function of the laser frequency.

Since the bands observed in the IRMPD of $V_6O_{15}{}^+$ spectrum are similar to the positions of the bands in the $V_4O_{10}{}^+$ spectrum, a similar assignment can be given. The first band at 876 cm^{-1} is assigned to the $V-O-V$ stretch and the second band at 1036 cm^{-1} to vanadyl stretch $V=O$.

In order to check the possibility of sequential fragmentation, the IRMPD spectrum of the $V_6O_{13}{}^+$ was measured from 600 to 1600 cm^{-1} (see Figure 6.8). A VO-loss dissociation channel is observed. The spectrum was measured with 0.05 μm step size. Higher resolution spectra with 0.02 μm step size were measured in the range of the

observed peak (see inset Figure 6.8). The spectrum reveals only one band at 890 cm^{-1} with a FWHM of 44 cm^{-1} and represents only 0.3% of the parent ions signal similar to the VO_3-loss in $V_6O_{15}{}^+$. The spectrum is identical to the VO_3-loss spectrum from Figure 6.8, supporting the assignment of a sequential decay mechanism. These experiments suggest that $V_6O_{15}{}^+$ has a structure that contains a $V_6O_{13}{}^+$ core with two O atoms attached to it. CID studies of Bell *et al.*[37] report two main dissociation channels for $V_6O_{13}{}^+$, namely V_3O_7-loss and V_5O_{12}-loss. No VO-loss is indicated by these experiments. Theoretical calculations are not available for this ion, however, based on previous spectra, the peak at 890 cm^{-1} can be assigned to the $V-O-V$ antisymmetric stretch.

DFT calculations on V_6O_{15} neutral were performed by Vyboishchikov and Sauer[169] indicating a cage like structure as in the case of V_4O_{10}, however, the predicted IR spectrum differs from the one presented here. The simulated spectrum reveals three intense bands in the region from 800 to 1100 cm^{-1}, whereas only two bands are observed experimentally.

In conclusion, the IR spectra of the $V_6O_{15}{}^+$ and $V_6O_{13}{}^+$ cations was measured between 600 and 1600 cm^{-1}. The spectral features were assigned based on the comparison with the spectrum of $V_4O_{10}{}^+$ to $V-O-V$ and $V=O$ stretches. No prediction of the structure can be made for $V_6O_{15}{}^+$ based on the DFT calculations on the neutral system, since the two spectra are different. However, based on the similarity of the $V_4O_{10}{}^+$ and $V_6O_{15}{}^+$ spectra and on the simplicity of the IRMPD spectrum presented here, a cage like structure with high symmetry is tentatively proposed as the absorbing specie.

6.2.6 Conclusions

In this section, the first successful IR spectra we performed at the FELIX facility were presented. The structure of selected oxygen rich vanadium oxide cationic clusters was probed by the IRMPD technique. For $V_4O_{10}{}^+$ the lowest lying isomer with a cage type structure was tentatively proposed as absorbing species. This tentative assignment is supported by the IRMPD spectrum of $V_4O_{12}{}^+$, but the CID background signal formed at the entrance in the trap through collision with the cold He atoms remains difficult to explain. Furthermore, IRMPD experiments performed on $V_3O_8{}^+$ suggest that the structure of two different isomers might be probed in the measurements. The IRMPD spectrum of $V_6O_{15}{}^+$ was measured as well. From the similarity of this spectrum with the IR spectrum of $V_4O_{10}{}^+$ a similar structure is tentatively proposed.

A definitive structural assignment to the measured spectra presented in this chapter is difficult without simulations of the IR spectra of these cations. Hopefully, the experimental studies presented here will stimulate future theoretical investigations on these systems.

Additional IRMPD spectra for $V_2O_3^+$ and $V_3O_2^+$ are shown in Appendix C.2. The understanding of these spectra require additional studies.